1-1-2011

Modification of Turbulence at the Air-Sea Interface Due to the Presence of Surfactants and Implications for Gas Exchange. Part II: Numerical Simulations

Silvia Matt
Nova Southeastern University, sm1424@nova.edu

Atsushi Fujimara
Nova Southeastern University, fujimura@nova.edu

Alexander Soloviev
Nova Southeastern University; University of Miami, soloviev@nova.edu

Shin Hyung Rhee
Seoul National University

Title	Gas Transfer at Water Surfaces 2010(p.299)
Author(s)	Hunt, J.; Belcher, S.; Stretch, D.; Sajjadi, S.; Clegg, J.; Kitaigorodskii, S.A.; Toba, Y.; Turney, D.; Banerjee, S.; Janzen, J.G.; Schulz, H.E.; Gonzalez, B.C.G.; Lamon, A.W.; Hughes, C.; Drennan, W.M.; Kiefhaber, D.; Balschbach, G.; Abe, A.; Heinlein, A.; Lee, G.A.; Jirka, G.H.; Kurose, R.; Waite, C.; Onesemo, P.; Ninaus, G.; Choi, Y.J.; Takahashi, K.; Baba, Y.; Komori, S.; Ohtsubo, S.; Takagaki, N.; Iwano, K.; Handa, K.; Shimada, S.; Akiya, Y.; Beya, J.; Peirson, W.; Banner, M.; Nezu, I.; Mizuno, S.; Sanjou, M.; Garbe, C.S.; Toda, A.; Takehara, K.; Takano, Y.; Etoh, T.G.; Caulliez, G.; Hung, L.-P.; Tsai, W.-T.; Tejada-Martínez, A.E.; Akan, C.; Khatiwala, S.; Grosch, C.E.; Jayathilake, P.G.; Khoo, B.C.; Rocholz, R.; Tan, Z.; Nicholson, D.P.; Leifer, I.; Emerson, S.R.; Hamme, R.C.; Mischler, W.; Simões, A.L.A.; Jähne, B.; Patro, R.; Loh, K.; Cheong, K.B.; Uittenbogaard, R.; Jeong, D.; Mori, N.; Nakagawa, S.; Soloviev, A.; Fujimura, A.; Gilman, M.; Hühnerfuss, H.; Monahan, E.C.; Haus, B.; Savelyev, I.; Matt, S.; Donelan, M.; Rhee, S.H.; Vlahos, P.; Huebert, B.J.; Edson, J.B.; Richter, K.E.; McNeil, C.L.; Yan, X.; Walker, J.W.; Zappa, C.J.; Ribas-Ribas, M.; McGillis, W.R.; Schimpf, U.; Rutgersson, A.; Nagel, L.; Orton, P.M.; D'Asaro, E.A.; Nystuen, J.A.; Gómez-Parra, A.; Forja, J.M.; Smedman, A.-S.; Sahlée, E.; Pettersson, H.; Kahma, K.K.; Perttilä, M.; Park, G.-H.; Chelton, D. B.; Bell, T.G.; Risien, C.M.; Kondo, F.; Suzuki, N.; Suzuki, Y.; Wanninkhof, R.; Johnson, M.T.; Campos, J.R.; Liss, P.S.; Tsukamoto, O.; Wanner, S.
Citation	Kyoto University Press. (2011)
Issue Date	2011-07-04
URL	http://hdl.handle.net/2433/156156
Right	Copyright (C) S. Komori, W. McGillis, R. Kurose, Kyoto University Press 2011
Type	Book
Textversion	publisher

Modification of turbulence at the air–sea interface due to the presence of surfactants and implications for gas exchange. Part II: Numerical simulations

Silvia Matt[1,2], Atsushi Fujimura[1], Alexander Soloviev[1,2] and Shin H. Rhee[3]

[1] *Oceanographic Center, Nova Southeastern University, 8000 N. Ocean Drive, Dania Beach, FL 33004, USA, Email: silvia.matt@nova.edu, fujimura@nova.edu, soloviev@nova.edu*

[2] *Rosenstiel School of Marine and Atmospheric Science, University of Miami, 4600 Rickenbacker Causeway, Miami, FL 33149, USA, Email: smatt@rsmas.miami.edu*

[3] *Department of Naval Architecture & Ocean Engineering, Seoul National University, 599 Gwanangno, Kwanak-gu, Seoul 151-744, Korea, Email: shr@snu.ac.kr*

Abstract. We conducted high-resolution non-hydrostatic numerical simulations to study the effect of surfactants on near-surface turbulence. Laboratory experiments at the UM RSMAS ASIST facility presented in a companion paper report a reduction of turbulence below the air-sea interface and an increase of the surface drift velocity in the presence of surfactants. We implement the effect of surfactants as a rheological, viscoelastic boundary condition at the surface. Our numerical experiments are consistent with the results of the laboratory experiments. We also simulated the effect of surfactants on the temperature difference across the thermal molecular sublayer (cool skin) and on gas transfer velocity. The numerical simulations demonstrate an increase in the temperature difference across the cool skin and reduction of the gas transfer velocity in the presence of surfactant. The results also reveal the effect of surfactants on the different types of molecular sublayers (viscous, thermal and diffusion), which is important for the development of proper parameterization of the interfacial component of air-sea gas exchange under low and moderate wind speed conditions.

Key Words: numerical simulation, LES, DES, CFD, viscoelastic boundary condition, rheology

1. Introduction

Surfactant films on the sea surface are an important factor in remote sensing. Reduced surface roughness can be observed in optical and radar images of the sea surface and can play a role in the visibility of small and fine-scale features on the sea surface (Alpers *et al*. 2010). Among these features are ship wakes, oil spills and natural slicks, fronts, eddies and internal waves. Wave energy dissipation mainly takes place in the boundary layer below the surface film. Damping effects on short surface waves and near-surface turbulence also have important

implications for gas transfer.

In this paper, we simulate the effect of surfactants on near-surface turbulence by using the state-of-the-art Computational Fluid Dynamics (CFD) software ANSYS FLUENT with an elastic boundary condition and with wind stress applied.

Section 2 of this paper describes the numerical model and techniques and discusses the model set-up and parameters. In Section 3, we present and discuss the results from our numerical simulations. Section 4 concludes the article.

2. Numerical model

In this section, we describe the numerical model as well as the model set-up and parameters. We use a high-resolution non-hydrostatic numerical model, the CFD software ANSYS FLUENT 12.1, to model the effect of surfactants on near-surface turbulence. FLUENT uses a control volume approach to solve conservation equations for mass and momentum. Here, we describe the theory for the Large Eddy Simulation (LES) and Detached Eddy Simulation (DES) turbulence models used in our simulations. In this article, we concentrate on the results from the LES simulations and will only present a summary of the DES results.

The governing equations for LES are obtained by filtering the time-dependent Navier-Stokes equations. The process filters out eddies with scales smaller than the filter width or grid spacing, and the resulting equations thus govern the dynamics of the large eddies (Sagaut 1998).

2.1. LES component

The governing equations for LES, obtained by filtering the time-dependent Navier-Stokes equations, in tensor notation are as follows:

$$\frac{\partial \rho}{\partial t}+\frac{\partial}{\partial x_i}(\rho \bar{u}_i)=0 \tag{1}$$

$$\frac{\partial}{\partial t}(\rho \bar{u}_i)+\frac{\partial}{\partial x_j}(\rho \bar{u}_i \bar{u}_j)=\frac{\partial}{\partial x_j}(\sigma_{ij})-\frac{\partial \bar{p}}{\partial x_i}-\frac{\partial \tau_{ij}}{\partial x_j} \tag{2}$$

where σ_{ij} is the stress tensor due to molecular viscosity defined by

$$\sigma_{ij}=\left[\mu\left(\frac{\partial \bar{u}_i}{\partial x_j}+\frac{\partial \bar{u}_j}{\partial x_i}\right)\right]-\frac{2}{3}\mu\frac{\partial u_l}{\partial x_l}\delta_{ij} \tag{3}$$

and τ_{ij} is the subgrid-scale stress defined by $\tau_{ij}\equiv\overline{\rho u_i u_j}-\rho\bar{u}_i\bar{u}_j$. (4)

2.2 LES-WALE

In the LES approach, the subgrid-scale stresses resulting from the filtering operation need to be modeled. In FLUENT, the subgrid-scale turbulent stresses are computed, using the Boussinesq hypothesis, from:

$$\tau_{ij}-\frac{1}{3}\tau_{kk}\delta_{ij}=-2\mu_t\bar{S}_{ij}\,, \tag{5}$$

where μ_t is the subgrid-scale turbulent viscosity. τ_{kk} is the isotropic part of the subgrid-scale stresses which is not modeled but added to the term containing the filtered static pressure. The rate-of-strain tensor for the resolved scales is

$$\bar{S}_{ij}=\frac{1}{2}\left(\frac{\partial\bar{u}_i}{\partial x_j}+\frac{\partial\bar{u}_j}{\partial x_i}\right). \tag{6}$$

FLUENT offers several models to calculate the turbulent viscosity μ_t, we chose the so-called Wall-Adapting Local Eddy-Viscosity (WALE) model (Nicoud and Ducros 1999).

In the WALE model, the eddy viscosity becomes

$$\mu_t=\rho L_s^2\frac{(S_{ij}^dS_{ij}^d)^{3/2}}{(\bar{S}_{ij}\bar{S}_{ij})^{5/2}(S_{ij}^dS_{ij}^d)^{5/4}}\,, \tag{7}$$

and L_s and S_{ij}^d are defined as follows

$$L_s=\min(\kappa d,\, C_wV^{1/3}) \tag{8}$$

$$S_{ij}^d=\frac{1}{2}(\bar{g}_{ij}^2+\bar{g}_{ji}^2)-\frac{1}{3}\delta_{ij}\bar{g}_{kk}^2,\ \bar{g}_{ij}=\frac{\partial\bar{u}_i}{\partial x_j} \tag{9}$$

Here, L_s is the mixing length for the subgrid scales, κ is the von Kármán constant, d is the distance closest to the wall and V is the volume of the computational cell; the local grid scale Δ is $V^{1/3}$. C_w is a constant and set to the default value of $C_w=0.325$.

Furthermore, the subgrid-scale turbulent flux of a scalar Φ is modeled via a subgrid-scale turbulent Prandtl number σ_t, calculating the subgrid-scale flux q_j as

$$q_j=-\frac{\mu_t}{\sigma_t}\frac{\partial\Phi}{\partial x_j}\,. \tag{10}$$

2. 3. DES

We also explored simulations using the Detached Eddy Simulation (DES) turbulence model. The DES model is a hybrid, which combines the Reynolds Averaged Navier-Stokes (RANS) model in the near-wall regions with Large Eddy Simulation (LES) in regions where the flow is separated from the boundary and

large-scale turbulence is dominant (Strelets 2001). In DES, a wider range of scales is modeled than in traditional LES, and RANS type models are often used to parameterize the subgrid-scale.

2.3.1 Realizable k-ε model

To model the subgrid-scale in DES, we have used the so-called realizable k-ε model (Shih *et al*. 1995), which is a RANS type model. The realizable k-ε model is a variation of the traditional k-ε model, where the eddy viscosity formulation is based on the mathematical constraints of realizability. These are that the normal Reynolds stresses be positive and that the Schwartz inequality must not be violated for the turbulent shear stresses (Schumann 1977; Shih *et al*. 1995). The realizable k-ε model is considered an improvement over the standard k-ε model.

The transport equations for the turbulent kinetic energy (k) and its dissipation rate (ε) in the tensor notation are as follows:

$$\frac{\partial}{\partial t}(\rho k)+\frac{\partial}{\partial x_j}(\rho k u_j)=\frac{\partial}{\partial x_j}\left[\left(\mu+\frac{\mu_t}{\sigma_k}\right)\frac{\partial k}{\partial x_j}\right]+G_k+G_b-\rho\varepsilon+S_k \tag{11}$$

$$\frac{\partial}{\partial t}(\rho\varepsilon)+\frac{\partial}{\partial x_j}(\rho\varepsilon u_j)=\frac{\partial}{\partial x_j}\left[\left(\mu+\frac{\mu_t}{\sigma_\varepsilon}\right)\frac{\partial \varepsilon}{\partial x_j}\right]+\rho C_1 S\varepsilon-\rho C_2\frac{\varepsilon^2}{k+\sqrt{v\varepsilon}} + C_{1\varepsilon}\frac{\varepsilon}{k}C_{3\varepsilon}G_b+S_\varepsilon \tag{12}$$

where

$$C_1=\max\left[0.43,\frac{\eta}{\eta+5}\right],\quad \eta=S\frac{k}{\varepsilon},\quad S=\sqrt{2S_{ij}S_{ij}}\,.$$

In equation (11), G_k represents the generation of turbulent kinetic energy due to the mean velocity gradients; G_b is the generation of turbulent kinetic energy due to buoyancy

$$G_b=\beta g_i\frac{\mu_t}{\mathrm{Pr}_t}\frac{\partial T}{\partial x_i}, \tag{13}$$

where β is the thermal expansion coefficient, g_i is the gravitational vector in direction i and Pr_t is the turbulent Prandtl number.

In the equations, $C_{1\varepsilon}$ and C_2 are dimensionless constants ($C_{1\varepsilon}=1.44$, $C_2=1.9$); μ and μ_t are the molecular and turbulent viscosity of water; σ_k and σ_ε are the turbulent Prandtl numbers for k and ε, respectively ($\sigma_k=1.0$, $\sigma_\varepsilon=1.2$). The user-defined source terms S_k and S_ε are set to zero in this study.

The eddy viscosity is computed as

$$\mu_t=\rho C_\mu\frac{k^2}{\varepsilon}, \tag{14}$$

where C_μ is a function of the mean strain and rotation rates, the angular velocity of the system rotation, and the turbulence fields (k and ε). The dependency of C_μ on the mean strain rate ensures realizability (Shih *et al*. 1995).

In DES, the RANS dissipation term in the k equation is then modified as follows

$$Y_k=\rho k^{3/2}/l_{DES}\,, \tag{15}$$

where

$$l_{DES}=\min(l_{RKE}, l_{LES}),\ l_{RKE}=\frac{k^{3/2}}{\varepsilon},\ \text{and}\ l_{LES}=C_{DES}\Delta;$$

C_{DES} is a calibration constant used in the DES model (which has a value of 0.61), and Δ is the maximum local grid spacing (Δx, Δy, Δz).

2.4 Heat and scalar transport

In the model, the equation for heat transport is solved as an energy equation, which in our case reduces to

$$\frac{\partial T}{\partial t}+\frac{\partial}{\partial x_i}(u_i T)=\frac{\partial}{\partial x_i}\left[(k+k_t)/(c_p\rho)\frac{\partial T}{\partial x_i}\right], \tag{16}$$

where T is the temperature, c_p is the specific heat capacity, k is the conductivity and k_t is the turbulent thermal conductivity according to the turbulence model used.

In addition, the equation for the conservation of an arbitrary scalar Φ is as follows:

$$\frac{\partial}{\partial t}(\rho\Phi)+\frac{\partial}{\partial x_i}(u_i\rho\Phi)=\frac{\partial}{\partial x_i}\left(\mu_c\frac{\partial\Phi}{\partial x_i}\right). \tag{17}$$

Here, μ_c is the molecular diffusion coefficient.

2.5 Boundary conditions

At the top of the domain, $z=0$ m, the boundary condition is that of a rigid lid with an applied shear stress of $\tau_0=0.02$ N m^{-2}. This stress corresponds approximately to 4 m s^{-1} wind speed at a 10 m height above the ocean.

In the presence of surfactant, the elastic surface boundary condition is then formulated as follows:

$$\tau_x=\tau_0+\frac{\partial\sigma}{\partial C}\frac{\partial C}{\partial x}+\frac{\partial\sigma}{\partial T}\frac{\partial T}{\partial x}, \tag{18}$$

$$\tau_y=\frac{\partial\sigma}{\partial C}\frac{\partial C}{\partial y}+\frac{\partial\sigma}{\partial T}\frac{\partial T}{\partial y}, \tag{19}$$

where the second term on the right hand side of (18) is determined by the elastic properties of the surfactant. Here, σ is the surface tension, *C is* the concentration of surfactant in the monolayer, and *T* is the sea surface temperature. The last terms on the right hand side of (18) and (19) represent the classical Marangoni effect due to dependence of the surface tension on temperature.

It is known that at high mean concentrations, the damping coefficient for naturally occurring surfactants such as oleic acid or oleyl alcohol is nearly constant (Ermakov 1996). Surfactants form a monomolecular film on the water surface with excess surfactant concentrated in microscopic droplets. Surfactant is continuously removed from the surface by renewal processes and resupplied from these surfactant "lenses". The saturated films then act like a monolayer completely covering the surface.

To our knowledge, this is the first study in which the effects of surfactant on near-surface fields have been studied using a boundary condition that allows for the inclusion of surface stress.

For the remaining boundaries, we specify free-slip boundary conditions at the bottom (z＝－0.5 m) and at the two lateral sides of our domain. At the "front" (x＝0 m) and "back" (x＝0. 5 m) sides of the domain, periodic boundary conditions are applied (Figure 1). The bottom of the domain and the non-periodic domain sides are insulated for temperature and a heat flux of -100 W m^{-2} is applied at the top.

2.6. Model Setup and Parameters

The model was run in parallel on 8 processors on two Dell Precision T7400 work stations with two Quad-Core Intel Xeon processors each and 64bit Windows XP operating system.

We used a pressure-based, 2nd order implicit solver and the LES and DES models as described above. We specified the material in our domain as water with a bulk temperature T＝293.15 K, density ρ＝998.2 kg m^{-3}, pressure p = 101325 Pa, and specific heat c_p＝4182 J $kg^{-1}K^{-1}$. Operating conditions were set to 20°C and atmospheric pressure (Table 1).

The model grid was generated with the FLUENT preprocessor Gambit. For LES, the grid consists of a square model domain of x＝0 m to x＝0.5 m and y＝－0.25 m to y＝0.25 m with Δx＝Δy＝0.0025 m in the horizontal (Table 2) (The domain for the DES simulations was slightly different, x＝0 m to x＝0.5 m and y＝－0.26 m to y＝0.26 m, and the horizontal resolution was Δx＝Δy＝ 0.0035 m). In the vertical, the domain ranges from z＝－0.5 m to z＝0 m (top) with Δz_{top}＝0.001 m. The grid resolution in the vertical was set to change from the top at a growth rate of R＝1.1 until Δz＝0.005 m is reached and then kept constant to the bottom of the domain at z＝－0.5 m. The time step is Δt＝0.05s for all

Table 1 Model physical parameters. Here: Pr = ν/κ is the Prandtl number and Sc = ν/μ is the Schmidt number.

Molecular kinematic viscosity ν $m^2\ s^{-1}$	Molecular heat diffusivity κ $m^2\ s^{-1}$	Molecular gas diffusivity μ $m^2\ s^{-1}$	Prandtl number Pr	Schmidt number Sc	Surface stress τ_0 $N\ m^{-2}$
$1.0819 \cdot 10^{-6}$	$1.4373 \cdot 10^{-7}$	$1.00 \cdot 10^{-7}$	7.5	10.8	−0.02

Table 2 Grid dimensions.

	Length, m	Width, m	Height, m	Δx, m	Δy, m	Δz, m	Growth Rate
Experiment	0.5	0.5	0.5	0.0025	0.0025	0.001	1.1

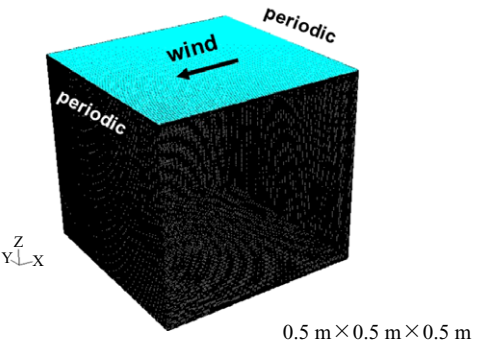

Figure 1 Model grid, indicating boundary condition and orientation of coordinate system.

simulations.

We spun up the model to steady-state for model time t＝600s before adding the surfactant boundary condition. Results are shown from time t＝800s.

3. Results and discussion

3.1 Effect of surfactants on near-surface turbulence

The presence of “streaks” (streamwise vortices) and coherent structures in turbulent boundary layers has previously been reported from both laboratory experiments and numerical simulations (Kim 1987; Lesieur 2008). We were able to reproduce such “streaks” and turbulent fluctuations below the water surface with the numerical model. The addition of an elastic boundary condition simulating the presence of surfactants at the water surface allowed us to investigate the effect of surfactants on the subsurface circulation.

A top view of the along-tank velocity field clearly shows “streak-like” features

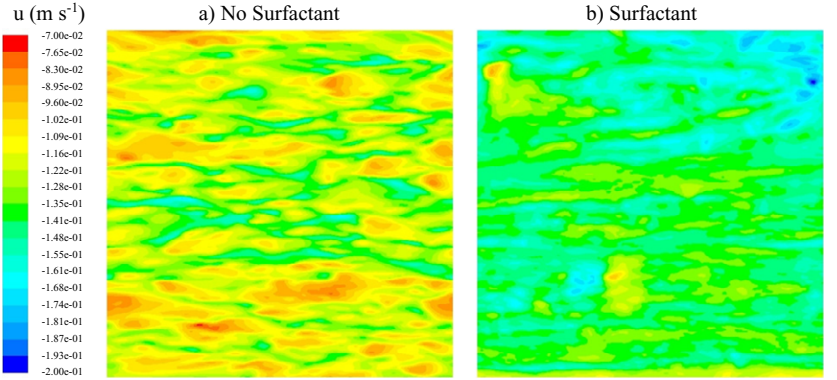

Figure 2 Top view of along-tank velocity without (a) and with (b) elastic boundary condition simulating surfactant effect.

(Figure 2a). With the addition of the surfactant boundary condition, a noticeable damping of these streaks occurs (Figure 2b).

A cross-section, taken in the center of the tank, of the along–tank velocity illustrates the circulation in the domain and the subsurface velocities, also affected by the surfactant boundary condition (Figure 3a, b). The near-surface circulation is less pronounced after the addition of the elastic boundary condition.

In a side view of the across-tank velocity, taken along the centerline of the tank, we observe Tollmien-Schlichting type, "ramp-like" structures near the surface (Figure 3c). These also appear to be suppressed by the surfactant effect (Figure 3d).

3.2 Effect of surfactants on near-surface turbulence and surface drift current

Figure 4 shows average current velocity profiles from the numerical simulations in comparison with results from the laboratory experiment described in the companion paper (Soloviev *et al*. this issue). The increase of the surface drift velocity observed in the presence of surfactants in the upper few centimeters of the water layer in the laboratory experiment (Figure 4a, b), is also seen in the numerical results (Figure 4c, d). As hypothesized in the companion paper referred to above, this may be the result of the suppression of turbulent velocity fluctuations and coherent structures (streaks and ramp-like structures) due to effects of the boundary (air-water interface) elasticity in the presence of surfactants.

Increase of the surface drift velocity is a consequence of the mixing suppression or, equivalently, reduction of the drag coefficient from the water side of the air-water interface. The respective reduction of the drag coefficient is described by the following formula:

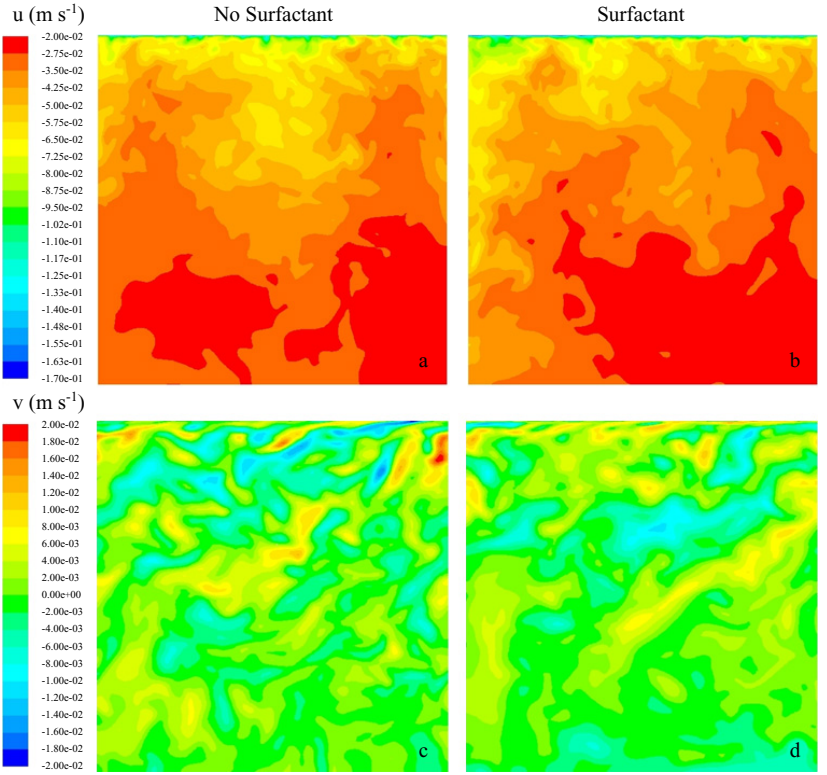

Figure 3 Top: Cross-sections of along-tank velocity (u) without (a) and with (b) elastic boundary condition show the circulation below the surface. Bottom: Side view of cross-tank velocity (v) show Tollmien-Schlichting type instabilities, without (c) and with (d) elastic boundary condition.

$$C_d/C_{ds} = (\Delta\bar{u}/\Delta\bar{u}_s)^2, \tag{20}$$

where $\Delta\bar{u}_s$ and $\Delta\bar{u}$ are the average velocity differences between 6 cm depth and the water surface with and without surfactant.

According to Table 3, in the presence of surfactants, the drag coefficient below the surface reduces by almost a factor of 2. The lab experiment of Soloviev *et al*. (this issue) showed a similar reduction of the drag coefficient by a factor of 1/0.64＝1.56. The difference may be explained by the fact that for the same wind speed, the addition of surfactant results in a reduction of the momentum flux at the air-water interface due to the drag reduction from the air side (see eq.4 and related text in Soloviev *et al*. this issue). This effect has not been accounted for in the numerical model.

The formulation of our surfactant boundary condition allows for the inclusion

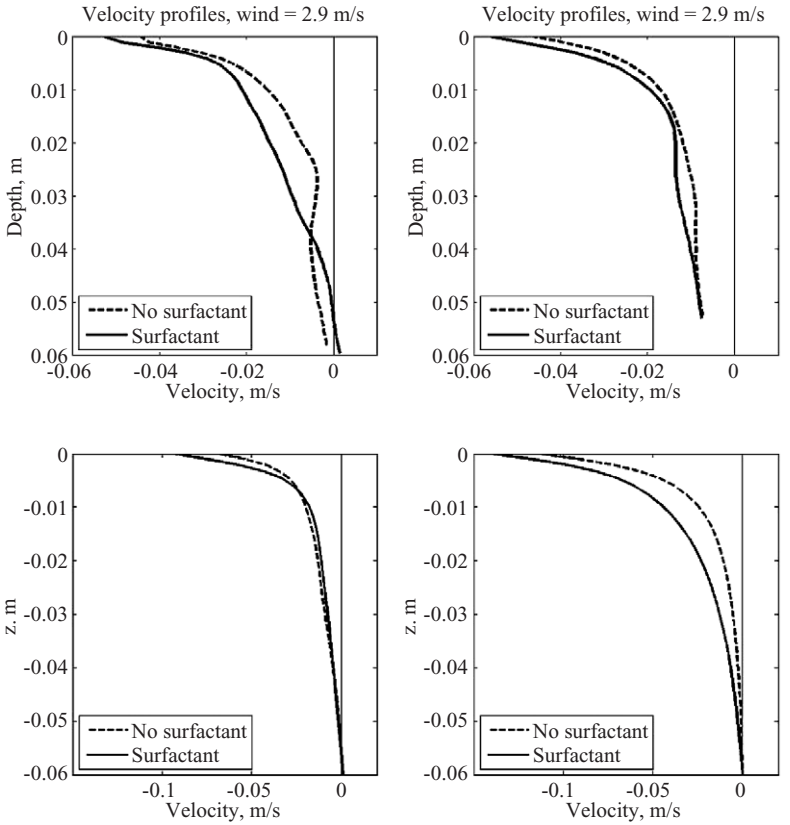

Figure 4 Along tank velocity (u) referenced to $z = -0.06$ m depth - laboratory data vs. CFD. Top: DPIV (Lab), two separate experiments (see Soloviev *et al*. 2010) with wind speed referenced to 10 m height, $U_{10} \approx 2.9$ m s^{-1}. Bottom: LES-WALE (left), DES with realizable k-ε (right). Note the increase in surface drift velocity in the presence of surfactant.

Table 3 Drag reduction under the water surface due to presence of surfactants.

C_d/C_{ds}	Temperature Marangoni off	Temperature Marangoni on
LES-WALE	1.8	1.9

of a Marangoni temperature coefficient. We investigate what impact the inclusion of this coefficient in the surfactant boundary condition has on the flow. The observed effect on the averaged vertical velocity and temperature profiles is very small (Figures 5, 6).

3.3 Application to the problem of air-sea gas transfer

Surface renewal theory results in the following relationships between the velocity and temperature differences in the aqueous viscous and thermal sublayers, and the gas transfer velocity for low soluble gases at the air-sea interface (Soloviev *et al*. 2007):

$$\Delta\bar{u}/u_* = \mathrm{Pr}^{-n}\Delta\bar{T}/T_* , \tag{21}$$

$$\Delta\bar{u}/u_* = A_0 Sc^{-n}u_*/K , \tag{22}$$

where $\Delta\bar{u}$ is the average velocity difference across the aqueous viscous sublayer, $\Delta\bar{T}$ is the average temperature difference across the aqueous thermal sublayer (cool skin), $T_* = Q_0/(c_p\rho u_*)$, and

$$K = G_0/\Delta\bar{C} \tag{23}$$

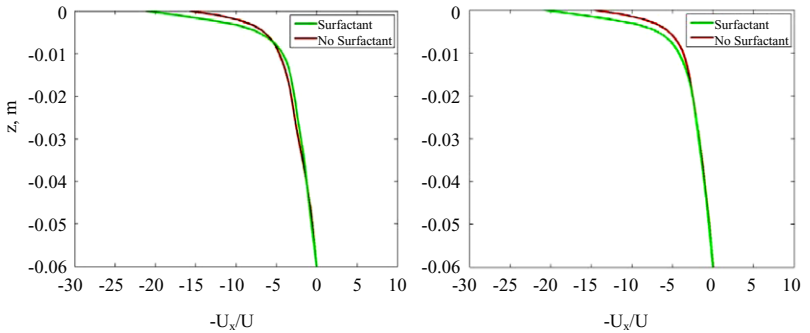

Figure 5 Effect of Marangoni temperature on velocity profiles - CFD
Marangoni temperature off (left), on (right).

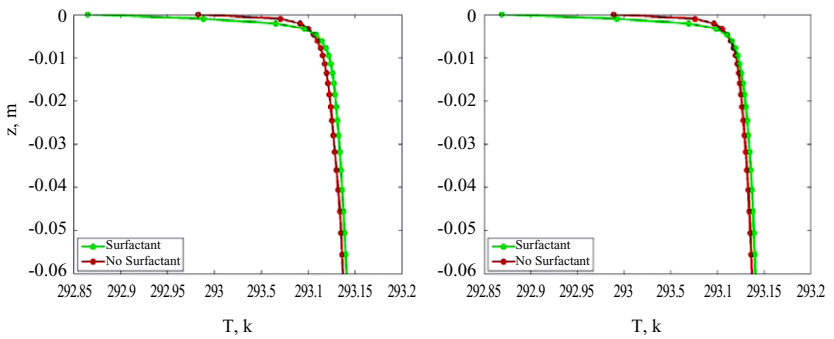

Figure 6 Effect of elastic boundary condition on temperature profiles - CFD
Marangoni temperature off (left), on (right)

is the gas transfer velocity; G_0 is the air-sea gas flux, $\Delta\overline{C}$ is the average gas concentration difference across the air-sea interface (which is localized in the aqueous diffusion sublayer for low soluble gases), and $A_0 \approx 1$ (Garbe *et al*. 2002). Pr and S_c are the Prandtl number and the Schmidt number, respectively; and $n = 1/2$.

Relationships (21)-(22) in the presence of surfactant can be rewritten as follows:

$$\Delta\overline{u}_s/u_* = \mathrm{Pr}^{-n_s}\Delta\overline{T}_s/T_* , \tag{24}$$

$$\Delta\overline{u}_s/u_* = A_0 Sc^{-n_s} u_* /K_s , \tag{25}$$

where subscript s denotes the presence of surfactant. From equations (21) and (24) it follows that:

$$n_s = 1/2 + \log[(\Delta\overline{u}/\Delta\overline{u}_s)/(\Delta\overline{T}/\Delta\overline{T}_s)]/\log \mathrm{Pr} \tag{26}$$

A similar relationship can also be obtained from equations (22), (23), and (25) as follows:

$$n_s = 1/2 + \log[(\Delta\overline{u}/\Delta\overline{u}_s)/(\Delta\overline{C}/\Delta\overline{C}_s)]/\log Sc \tag{27}$$

Table 4 summarizes the result of calculations using formulas (26), (27) and data shown in Figures 5-7.

From Table 4 it appears that the CFD results support the value of the exponent

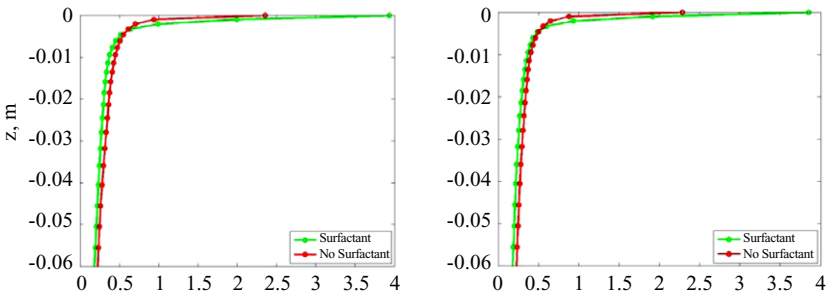

Figure 7 Effect of surfactant on the concentration of a passive tracer - CFD. Concentration scale is in technical units. Marangoni temperature off (left), on (right).

Table 4 Estimation of the exponent n_s in the presence of surfactant.

n_s	Temperature Marangoni off	Temperature Marangoni on
From Eq. (26)	0.64	0.61
From Eq. (27)	0.61	0.60

n_s=2/3 previously reported in a laboratory experiment by Jähne *et al.* (1987).

4. Conclusions

The results presented in this work from numerical modeling using the CFD code ANSYS FLUENT with a boundary condition simulating the presence of surfactants at the sea surface are qualitatively consistent with the lab experiment presented in a companion article (Soloviev *et al*. 2010). We have been able to reproduce the effect of suppression of near-surface turbulence due to the presence of surfactants, reduction of the drag coefficient, and respective increase of the surface drift current. The streaks, which are found in the buffer zone between the viscous sublayer and the core of the turbulent flow, have also been reproduced in our numerical simulations.

A mechanism for the damping effect of surfactants on the subsurface circulation is discussed in the companion paper (Soloviev *et al*. 2010). As surfactant accumulates in convergence zones on the water surface, the film stress is directed outward of these convergence zones. The converse is true for divergence zones with lower surfactant concentration. Overall, we see a suppression of the velocity divergences in the near-surface layer of the water. Using an elastic boundary condition simulating the presence of surfactants, we observe an increase of the surface drift velocity, an increase of the temperature difference across the cool skin, as well as a reduction of the gas transfer coefficient. The exponent in the dependence of the gas transfer velocity on the Schmidt number in the presence of surfactants is close to 2/3, a value previously reported from laboratory experiments. The two turbulence models used in this study, DES (with realizable k-ε) and LES-WALE, have produced somewhat different results. The LES-WALE model appears to be more robust. Validation and tuning of the numerical model using laboratory observations appear to be critical in the development of a realistic numerical model for the effect of surfactants on the near surface dynamics.

Acknowledgments

This work is a part of the NSU OC project “Hydrodynamics and Remote Sensing of Far Wakes of Ships”. We thank Dr. Mikhail Gilman for help with the implementation of user-defined functions (UDF) in the numerical model and for useful discussions.

References

Alpers,W., L. Mitnik, L. Hock, and K.S. Chen (1999), *The Tropical and Subtropical Ocean Viewed by ERS SAR*. Accessed 24 July 2010, at http: //www. ifm. zmaw.

de/fileadmin/files/ers-sar.

Ansys Fluent 12.1 (2010), Fluent User's Guide. *http://www.fluent.com/*.

Garbe, C.S., B. Jähne, and H. Haussecker (2001), Measuring sea surface heat flux and robability distribution of surface renewal events. In AGU Monograph *Gas Transfer at Water Surfaces*, (Eds: E.S. Saltzman, M. Donelan, W. Drennan, and R. Wanninkhof), 109-114.

Jähne, B., K.O. Muennich, R. Rosinger, A. Dutzi, W. Huber, and P. Libner (1987), On the parameterization of air-water gas exchange. *J. Geophys. Res., 92*, 1937-1949.

Kim, J., P. Moin, and R. Moser (1987), Turbulence statistics in fully developed channel flow at low Reynolds number. *J . Fluid Mech.*, *177*, 133-166.

Lesieur, M. (2008), *Turbulence in Fluids*, Fourth Revised and Enlarged Edition, Springer.

Nicoud, F. and F. Ducros (1999), Subgrid-scale stress modelling based on the square of the velocity gradient tensor. *Flow, Turbulence and Combustion*, *62*, 183-200.

Sagaut, P. (1998), *Large Eddy Simulation for Incrompressible Flows, An Introduction*. Springer.

Schumann, U.(1977), Realizability of Reynolds-stress turbulence models. *Phys. Fluids*, *20*, 721-725.

Shih, T.-H., W. W. Liou, A. Shabbir, Z. Yang, and J. Zhu (1995), A New k-ε Eddy-Viscosity Model for High Reynolds Number Turbulent Flows - Model Development and Validation. Computers&Fluids, *24*(3), 227-238.

Soloviev, A.V. (2007), Coupled renewal model of ocean viscous sublayer, thermal skin effect and interfacial gas transfer velocity. *Journal of Marine System, 66*, 19-27.

Soloviev, A. V., S. Matt, M. Gilman, H. Hühnerfuss, B. Haus, D. Jeong, I. Savelyev and M. Donelan (2010), Modification of Turbulence at the Air-Sea Interface Due to the Presence of Surfactants and Implications for Gas Exchange. Part I: Laboratory Experiment. *This issue*.

Strelets, M. (2001), Detached Eddy Simulation of Massively Separated Flows. AIAA 2001-0879, *39th AIAA Aerospace Sciences Meeting and Exhibit*, Reno, NV.